Preprint Title Modification of cellulose materials from *Borassus flabellifer* fruit husk for nickel recovery from spent lithium-ion batteries

Authors Khoa D. Pham-Nguyen, Bao V. P. Nguyen, Quan V. M. Do, Quang N. Tran, Huu-Quang Nguyen, My-Chi Nguyen, Jaebeom Lee and Hai S. Truong-Lam

Publication Date 17 Feb. 2025

Article Type Full Research Paper

ORCID® iDs Huu-Quang Nguyen - https://orcid.org/0000-0002-8609-3038; Hai S. Truong-Lam - https://orcid.org/0000-0003-2435-6039

Modification of cellulose materials from *Borassus flabellifer* fruit husk for nickel recovery from spent lithium-ion batteries

Khoa Dang Pham-Nguyen[1, 2], Nguyen Vinh Phuc Bao[1, 2], Do Viet Minh Quan[1, 2], Quang Nhat Tran[1, 2], Huu-Quang Nguyen[3], My-Chi Nguyen[3], Jaebeom Lee[3], Hai Son Truong-Lam[1, 2*]

[1]Faculty of Chemistry, University of Science, Ho Chi Minh City 70000, Vietnam

[2]Vietnam National University, Ho Chi Minh City 70000, Vietnam

[3]Department of Chemistry, Chungnam National University, Daejeon 34134, Republic of Korea

*Corresponding author.

E-mail address: Hai Son Truong-Lam - tlshai@hcmus.edu.vn

Abstract

This study explores the efficacy of carboxylated cellulose nanocrystals (M-CNCs) derived from *Borassus flabellifer* fruit husk as a sustainable adsorbent for the removal of nickel ions (Ni^{2+}) from aqueous solutions. M-CNCs were synthesized through a multistep process: microcrystalline cellulose extraction, nanocrystal isolation, and nanocrystal carboxylation. The response surface methodology was used to optimize Ni^{2+} adsorption through a systematic evaluation of its influencing parameters. The M-CNCs were characterized using Fourier-transform infrared spectroscopy, Brunauer–Emmett–Teller surface area analysis, and field-emission scanning electron microscopy, which confirmed the successful modification and structural integrity of the nanocrystals. The Ni^{2+} adsorption capacity of the M-CNCs was assessed under varying experimental conditions, including pH, temperature, adsorbent mass, and initial Ni^{2+} concentration. Kinetic studies revealed that the adsorption process followed the pseudo-second-order model, suggesting that chemisorption was the rate-limiting step. Notably, the M-CNCs demonstrated a selective affinity for Ni^{2+} ions in a synthetic battery solution, achieving an adsorption yield of approximately 70%. Thus, the M-CNCs possess significant potential for Ni^{2+} recovery from electronic waste and for wastewater treatment applications.

Keywords: carboxylated cellulose nanocrystals; response surface methodology; *Borassus flabellifer* fruit husk; spent lithium-ion batteries; electronic waste.

Introduction

The dramatic rise in the use of lithium-ion batteries (LiBs) in electronic devices necessitates proper recycling to minimize their environmental impact and maximize resource utilization [1]. LiBs contain heavy metals, particularly nickel, which can severely pollute the environment and significantly harm human health and ecosystems if not disposed of responsibly. Therefore, LiBs recycling, with a primary focus on the recovery of nickel and rare-earth metals, is a global imperative. This mitigates environmental damage while ensuring a sustainable supply of raw materials for the production of new batteries, thereby contributing to the sustainable development of the battery industry. Unlike conventional solid waste, electronic waste (e-waste) requires specialized preliminary treatments because of its intricate composition. Pyrometallurgical, bio-hydrometallurgical, and hydrometallurgical methods are frequently used to recover valuable metals from spent LiBs. However, pyrometallurgical processes demand sophisticated machinery, and biohydrometallurgical methods, albeit environmentally benign, have limited applicability due to their specific operational constraints [2]. Hydrometallurgy is less energy intensive than pyrometallurgy but generates liquid waste that requires further treatment [3]. Therefore, the pursuit of cost-effective, environmentally friendly methods is ongoing. One promising approach involves extracting environmentally friendly material, especially cellulose, from natural sources and modifying it to absorb the target metal, in this case nickel.

Bio-adsorbents derived from cellulose-rich agricultural by-products are environmental-friendly and readily available natural materials for metal removal from e-waste [4–6]. The biopolymer cellulose is a linear polysaccharide composed of β-D-glucopyranose units ($C_6H_{12}O_6$). Each unit contains three equatorial hydroxyl groups, which can be easily modified using appropriate substituents to create materials that can adsorb target metals. Recent studies have demonstrated the potential of various agricultural wastes, such as tea leaf fiber [9], sugarcane straw [11], rice husk [13], banana peel [15,16], corn stalk [17], and peanut shell [18], as cellulose sources. However, the valorization of *Borassus flabellifer* fruit husk (BFFH), a readily available agricultural waste in South Asia and Southeast Asia [19–21], particularly in regions such as An Giang Province, Vietnam, remains largely untapped.

Approximately 10.5 tons of BFFH are discarded daily in An Giang alone, according to the Statistics Office of Tinh Bien Town (2023). However, despite its abundance, its primary uses remain limited to fuel and fertilizer applications. Boopathi et al. [22] obtained a cellulose content of up to 68.94% after kernel extraction in a process aligned with the principles of green chemistry.

Several methods have been used to prepare CNCs, including enzymatic hydrolysis, 2,2,6,6-tetramethylpiperidinyloxy (TEMPO) oxidation, and mechanical methods. Cui et al. [25] and Filson et al. [26] used CNCs prepared from commercial MCC and recycled pulp, respectively. However, enzymatic hydrolysis requires using specific enzymes suitable for CNCs production and considering the enzyme dosage. Furthermore, this method often entails extended reaction times. TEMPO oxidation, albeit effective, needs pH control, necessitates multistep posttreatment, and generates by-products that can harm the environment and living organisms [27–29]. Ball milling is also a promising mechanical approach to CNCs preparation. However, when used alone, it typically results in CNCs with relatively high length and width dimensions. To address this limitation, ball milling is often conducted as a pretreatment step before acid hydrolysis, which helps to overcome the limitations of CNCs produced only through mechanical means [25,30,31].

In most traditional production or modification procedures, one factor (variable) is altered while others are kept constant [34]. However, it is common for chemical processes to involve numerous factors and require simultaneous assessment of potential interactions between multiple factors. Statistical experimental design methodologies, such as response surface methodology (RSM), have emerged as a solution to these limitations. A powerful combination of mathematical and statistical techniques, RSM is widely used to optimize processes and understand the interplay between experimental variables, thus improving overall outcomes [35,36]. By employing RSM, researchers can significantly reduce the number of required experiments while gaining a more comprehensive understanding of the analyzed process and identifying optimal conditions.

In this study, native cellulose were isolated from pretreated BFFH and subjected to acid hydrolysis to produce CNCs. The obtained CNCs were subsequently chemically modified via an RSM-optimized process to obtain carboxylated cellulose. The physicochemical properties of the resulting adsorbent were comprehensively characterized using Fourier-transform infrared spectroscopy (FT-IR), Brunauer–Emmett–Teller (BET) surface area analysis, and field-emission scanning electron microscopy (FE-SEM). The adsorption capacity of the prepared adsorbent for nickel ions (Ni^{2+}) was evaluated under varying conditions, including pH, adsorbent mass, and contact time. Furthermore, we performed kinetic studies and adsorption isotherm to describe the adsorption of Ni^{2+} by the processed M-CNCs materials. Through this comprehensive study, we aim for the utilization of agricultural waste materials such as BFFH for effective use of raw products and contribute towards green and sustainable economic developments.

Results and Discussion

Perspectives in pretreatment and preparation of the CNCs from *Borassus flabellifer* fruit husk

Pioneering research and applications that leverage BFFH as a source of novel compounds have contributed to waste reduction and opened new avenues in the development of sustainable materials. This study is a significant step toward identifying and utilizing environmentally friendly alternative raw materials. Due to the limitations of mechanical techniques (time consuming and requiring high pressure and energy) and enzymatic methods (laborious and reliant on microbial activity), chemical methods are currently favored, either independently or in combination with other techniques, for efficient cellulose isolation [23]. Thus, in this study, a chemical approach was utilized due to its simplicity and cost-effectiveness (**Figure 1)**. Before cellulose nanocrystals (CNCs) extraction, the source material is pretreated to remove impurities and extract native cellulose from the biomass. These include alkaline treatment, which solubilizes hemicelluloses and pectins while partially depolymerizing lignin; and bleaching to remove contaminants such as small organic molecules and chromophores. Bleaching with chlorine-based chemicals (chlorine and chlorine dioxide) is effective and economical [24] but generates

chlorolignins, which are resistant to biodegradation, and other potentially toxic pollutants. Therefore, hydrogen peroxide (H_2O_2) is used in this study for bleaching, as its sole by-product is water.

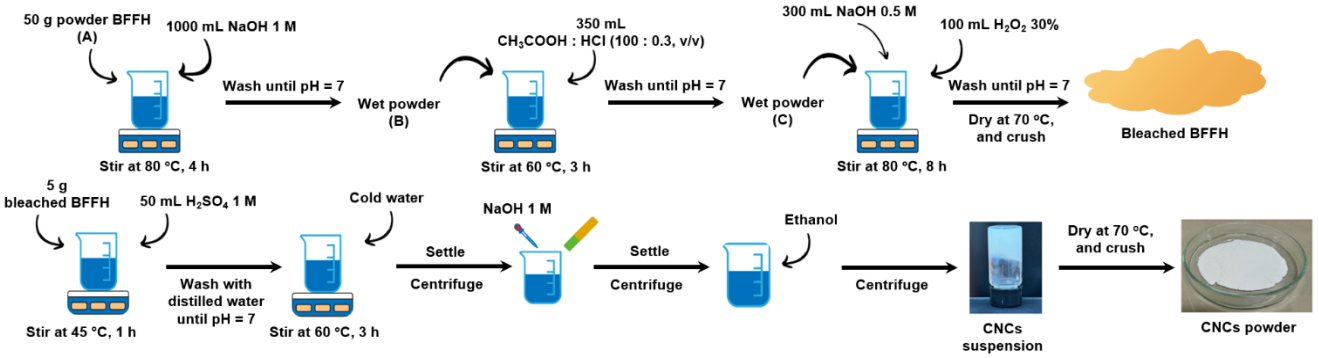

Figure 1: Cellulose nanocrystal extraction process from *Borassus flabellifer* fruit husk.

Nanocellulose is considerably more advantageous than microcrystalline cellulose (MCC) in metal extraction from waste materials, because it has a significantly larger surface area and thus better physical and chemical properties [23]. Sulfuric acid hydrolysis is the most common and widely used CNCs isolation method. It is simple and imparts a high negative surface charge to CNCs through the attachment of sulfonate ions to surface hydroxyl groups. This negative charge stabilizes CNCs in water, improving their handling properties. Consequently, sulfonated CNCs are extensively used to produce polymer nanocomposites with water-soluble polymers, such as poly(vinyl alcohol), carboxymethyl cellulose, chitosan, carrageenan, alginate, poly(ethylene oxide), and polylactic acid [32].

Unmodified cellulose exhibits limited heavy metal adsorption capacity and variable physical stability [33]. Therefore, chemical modification is necessary to enhance its structural durability and adsorption capacity. In this study, an oxidation reaction is induced using sodium nitrite and nitric acid to introduce carboxyl groups onto the C6 position of the glucose units in CNCs, thereby modifying their surface properties without altering their fundamental structure.

Fourier transforms infra-red spectroscopy

FT-IR analysis revealed the key spectral features of the samples. All samples exhibited a broad absorption band at 3000 – 3500 cm^{-1}, characteristic of O–H stretching vibrations in cellulose, and a peak at 2900 cm^{-1}, which was attributed to the C–H stretching vibrations of the alkyl group (**Figure 2**). The boiled sample displayed a peak at 1750 cm^{-1}, indicating the presence of carbonyl groups (C=O) from

hemicellulose acetyl esters [37]. However, this peak disappeared after the bleaching process, confirming the effectiveness of hemicellulose removal. Accordingly, the cellulose content increased to 88.37% ± 0.06% after bleaching, with cellulose yields of 30.76% ± 0.01%, aligning with TCVN 11921-1:2017 standards. This result was comparable to that of Wardani et al. [38], who adopted a microwave-assisted method to achieve a cellulose content of 74%, yielding a maximum cellulose yield of 29.82%.

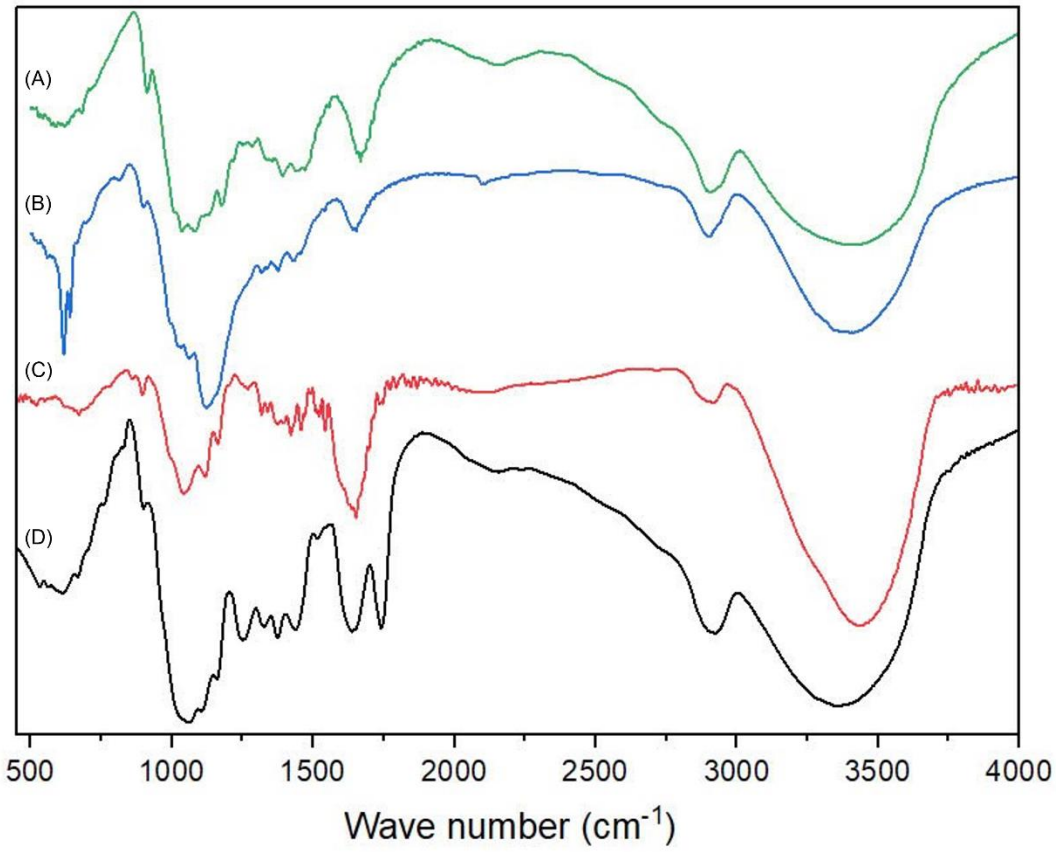

Figure 2: FT-IR spectra of carboxylated cellulose nanocrystal (A), cellulose nanocrystal (B), bleached *Borassus flabellifer* fruit husk (C), and heat-treated *Borassus flabellifer* fruit husk (D).

Analysis of the M-CNCs revealed a broader O–H absorption band compared with that in the bleached BFFH, suggesting increased hydrogen bonding between the cellulose chains. Notably, the O–H peak shifted to a higher wavenumber (3400 cm^{-1}) and increased in intensity, likely because hydrogen bonding was disrupted by the conversion of the primary hydroxyl groups at C6 to carboxyl groups [39,40].

C–O–C vibration, typically observed at 1028 cm^{-1}, exhibited splitting at 1018 and 1065 cm^{-1} in the M-CNCs, accompanied by an intensity reduction. This suggested alterations in the sum and difference of C–O vibrations between adjacent hexose rings, possibly caused by glycosidic bond cleavage and chain breakage [40,41]. Furthermore, the FT-IR spectrum of the M-CNCs displayed a characteristic peak at 1653 cm^{-1}, confirming the presence of a carboxylated group (C=O) in the form of sodium salt (–COONa) [41,42]. The boiled BFFH, bleached BFFH, and CNCs showed weak absorption signals at 1640 cm^{-1}, attributed to the O–H bending of adsorbed water [32,43,44].

In summary, FT-IR analysis effectively verified the successful removal of hemicellulose and the successful introduction of carboxyl groups (–COOH) onto the surface of the M-CNCs material.

FE-SEM and BET analysis

According to the FE-SEM results, the commercial MCC had a size range of 30 – 50 μm (**Figure 3A**), whereas the produced CNCs were needle-shaped nanoparticles with longitudinal size of 120 – 200 nm (**Figure 3B**). The CNC samples were thoroughly dispersed in water prior to drop-casting on a clean Si wafer for FE-SEM analysis. During the drying process, well-defined CNCs tend to undergo cholesteric self-assembly into liquid crystalline structures. The formation of uniform rod-like particles in the SEM images indicates that the chemical extraction and surface modification process resulted in CNCs with high quality and purity. These results demonstrated the removal of amorphous substances and the cleavage of the crystalline microfibrils of the MCC degraded into nanofibers. Moreover, the specific surface area of the M-CNCs was determined through the BET method. According to material property analysis, the BET specific surface area, specific pore volume, and average pore size were 0.729 $m^2\ g^{-1}$, 0.0002 $cm^3\ g^{-1}$, 1.152 nm, respectively. The M-CNCs had a smaller surface area than the CNCs [45] due to the CNCs drying process under the effect of heat, which decreased the contact ability of Ni^{2+}

ions on the material surface [46]. Therefore, the sample drying method significantly affected the specific surface area of the material, consistent with the findings of Beck et al. [47].

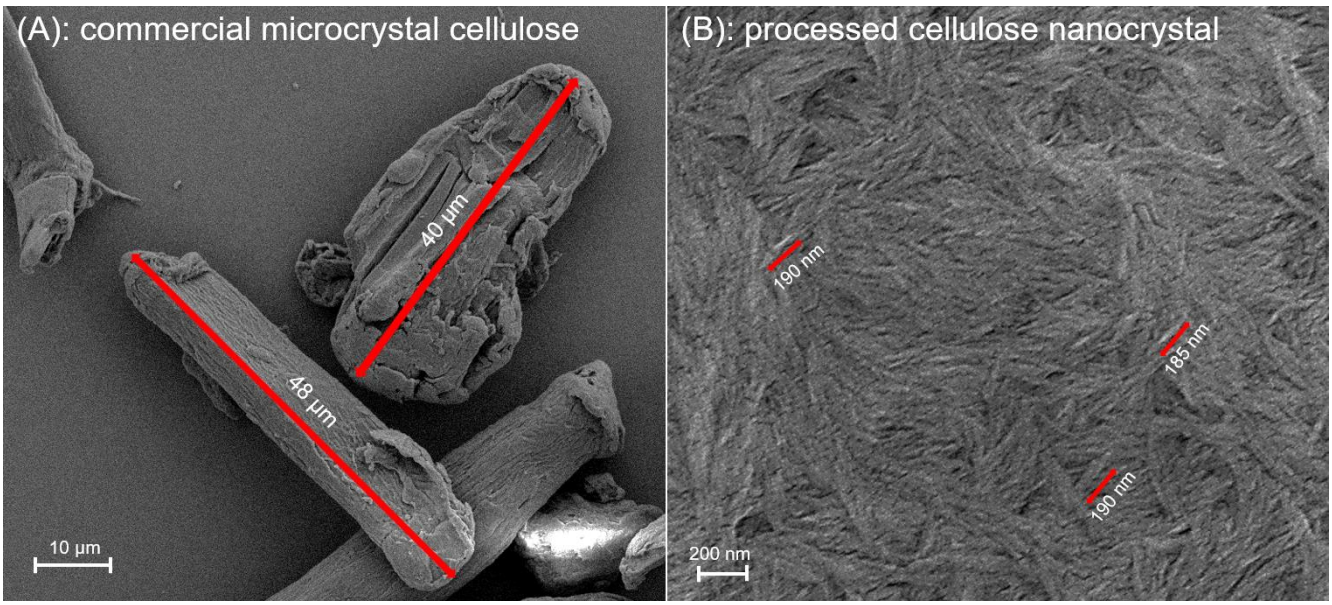

RSM in CNCs modification

Screening experiments revealed three factors significantly influencing Ni^{2+} adsorption efficiency: the CNCs amount, $NaNO_2$:HNO_3 volume ratio, and $NaNO_2$ volume. These were investigated and predicted using a more specialized model than the CCF one to select the optimal experimental conditions.

Three-dimensional plots were constructed to understand the interaction effect of the experimental variables on the Ni^{2+} removal percentage (**Figure 4**). Combination of the correlation data between the influencing factors indicated that the optimal conditions for CNCs surface modification were as follows: m_{CNCs} = 3 g, $t_{stirring}$ = 1 h, V_{NaNO_2}:V_{HNO_3} = 5:1, and V_{NaNO_2} = 22.5 mL. This resulted in a 93.7% Ni^{2+} removal efficiency. Three replicate experiments were conducted using the predicted optimal conditions to verify the accuracy of the CCF model. The average Ni^{2+} removal rate was 90.9% ± 1.0%, which differed from the predicted value by only 2.8%. Therefore, the RSM–CCF model demonstrated good predictive capability, so it was used to investigate the conditions of the influencing factors, especially in the optimization of CNCs surface modification.

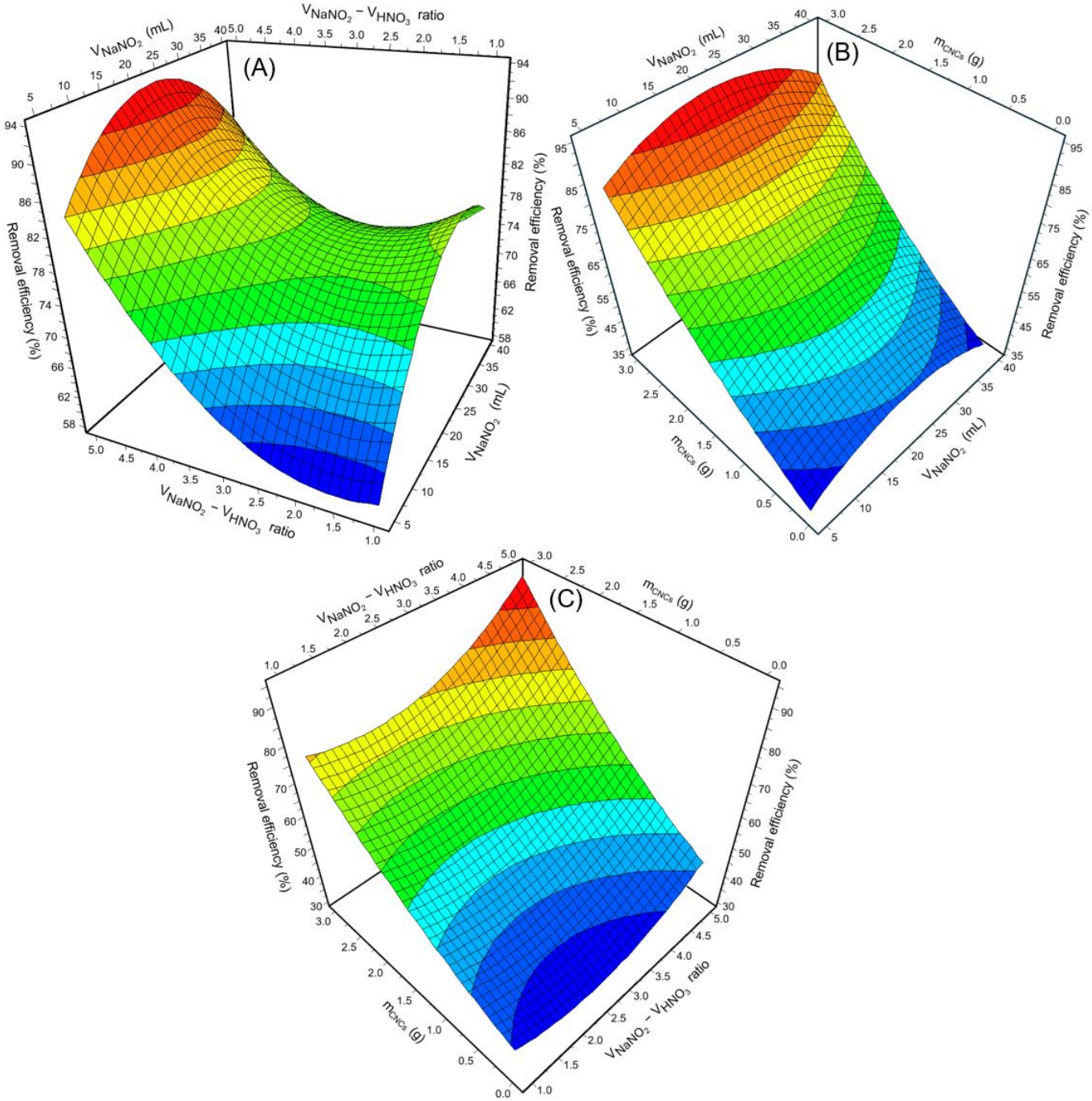

Figure 4: 3D graphs of removal efficiency percentage (H%) with interactions between independent variables: V_{NaNO_2}:V_{HNO_3} ratio and V_{NaNO_2}(mL) (A); V_{NaNO_2}(mL) and m_{CNCs} (g) (B); m_{CNCs} (g) and V_{NaNO_2}:V_{HNO_3} ratio (C).

Factors affecting Ni^{2+} adsorption

pH values

The treatment process, particularly the removal of metal ions from water, is greatly influenced by the solution pH. Due to variations in the type of metal ions existence and the adsorbent's surface charge density, pH fluctuations affect the metal removal process [48]. **Figure 5** illustrates the adsorption of Ni^{2+} using M-CNCs at pH values ranging from 1 to 9. A possible reason was that the pH of the analyzed adsorbent material depended on the protonation of the carboxylated groups on the material surface, forming an acid form (–COOH) [49]. Additionally, the adsorbent and Ni^{2+} interacted through electrostatic repulsion, which prevented Ni^{2+} ions from adhering to the material surface. This competitive adsorption between the metal cations and H^+ ions decreased with an increase in pH because –COOH readily dissociates and exists as $–COO^–$ [50]. Furthermore, a high pH solution caused the material surface to become more negatively charged, heightening the electrostatic attraction between the adsorbent and Ni^{2+} and increasing the adsorption of Ni^{2+} ions. The optimal removal efficiency was achieved at pH = 7 because of the negative charge density caused by the deprotonation of the carboxyl group ($–COO^–$) under neutral conditions. However, increasing the pH beyond 7 would cause the precipitation of Ni^{2+} hydroxide, affecting the adsorption efficiency [51]. The above analysis results highlighted the pH-dependent properties of the M-CNCs in removing Ni^{2+}. The pH was set to 7 for the following experiments.

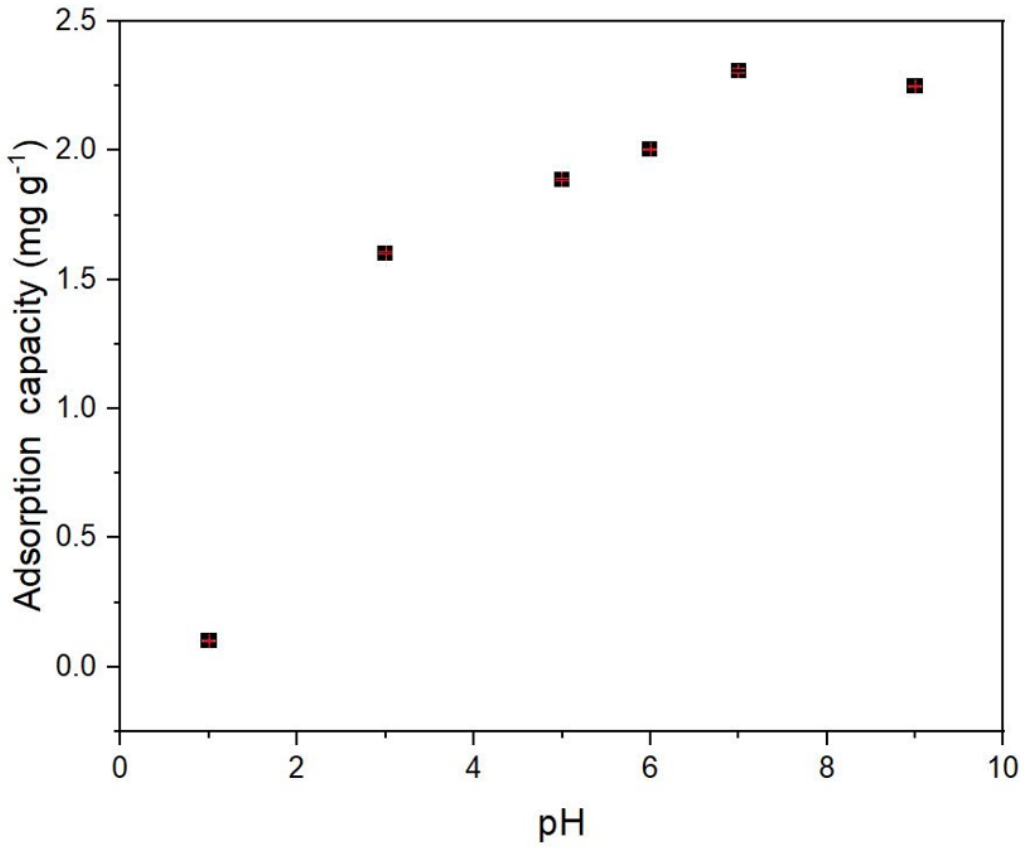

Figure 5: Effects of solution pH on removal of trace metals from aqueous solution (adsorbent dose = 100 mg, initial Ni^{2+} concentration = 10 mg L^{-1}, and volume = 25 mL). The square plots indicate adsorption capacity at different pH values.

Adsorbent mass

The absorbent mass required to attain the highest treatment efficiency while minimizing waste was determined. Adsorption experiments were conducted at pH = 7 at an initial Ni^{2+} concentration of 10 mg L^{-1} and M-CNCs masses of 0.02 – 0.2 g to examine the effect of the adsorbent mass on Ni^{2+} removal in water. As shown in **Figure 6**, the treatment efficiency reached 58.86% when the adsorbent mass was 0.02 g. When the mass increased to 0.2 g, efficiency almost reached 90% due to the increased surface area of the adsorbent and the presence of additional adsorption sites. However, when the adsorbent mass increased from 0.1 g to 0.2 g, the treatment efficiency increased by no more than 10%. Conversely, the Ni^{2+} adsorption capacity per unit mass of adsorbent decreased from 7.11 to 0.98 mg g^{-1}. The reason for these experimental results was that the higher adsorbent mass provided more adsorption sites, so these

sites were not saturated during adsorption. Furthermore, material diffusion and agglomeration decreased due to the interaction of polar groups (–OH^-, –COO^-, etc.) on the material surface. Ni^{2+} was less accessible to the available adsorption sites on the adsorbent surface because of the reduced overall adsorption surface area and the increased diffusion path length. Because the total treatment cost is closely related to the adsorbent cost, treatment efficiency and the amount of absorbent to be optimized should be balanced for the treatment process. Therefore, an adsorbent mass of 0.1 g, which was considered sufficient for Ni^{2+} removal, was selected for the subsequent experiments.

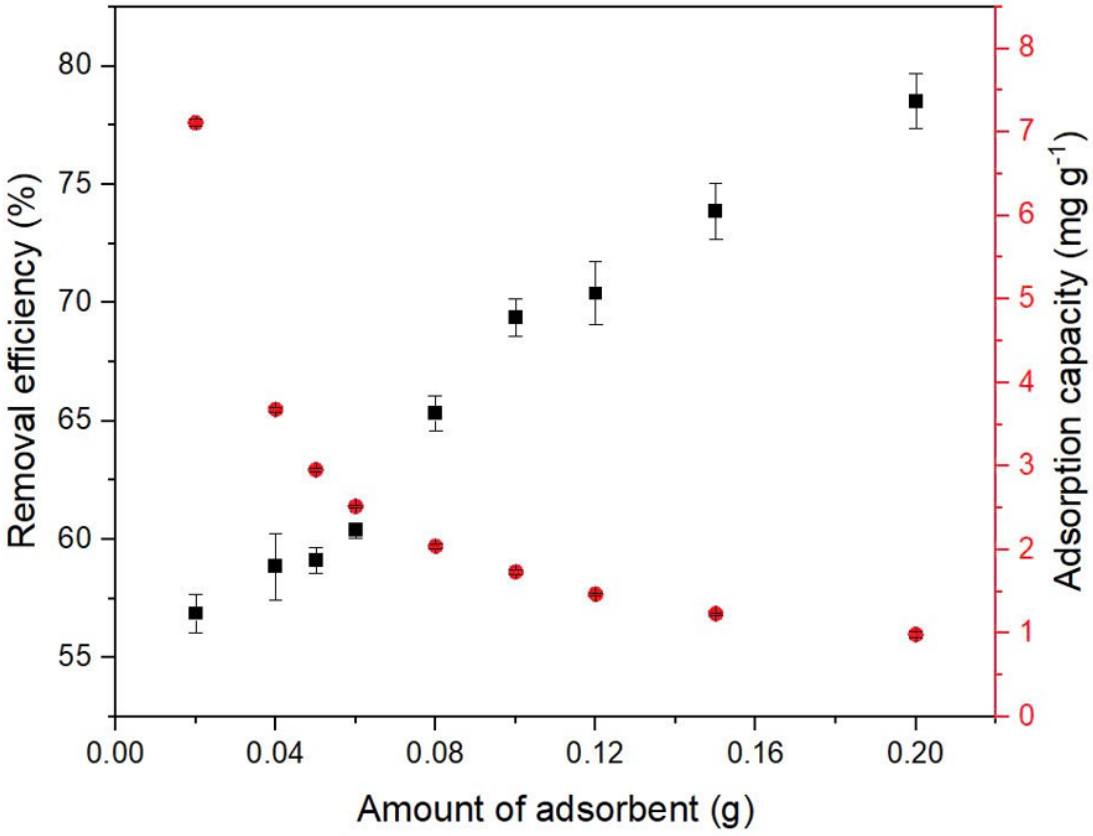

Figure 6: Effects of Carboxylated Cellulose Nanocrystal dosage on Ni^{2+} removal from aqueous solution (initial Ni^{2+} concentration = 10 mg $L^{-}1$, pH = 7, and volume = 25 mL). The square and circle plots represent adsorption capacity and removal efficiency, respectively, at different adsorbent amounts.

Adsorption time

The adsorption time plays a vital role in evaluating adsorption performance. It helps determine the maximum rate at which solutes can be effectively removed from a substance. The effect of the contact

time on the adsorption capacity of Ni^{2+} ions in the solution was studied using 0.1 g of adsorbent in 25 mL of a Ni^{2+} solution with initial Ni^{2+} concentrations of 10, 20, and 40 mg L^{-1}. When the starting concentration of the Ni^{2+} solution rose from 10 to 40 mg L^{-1}, the equilibrium adsorption capacity of the M-CNCs increased from 1.73 mg g^{-1} to 9.13 mg g^{-1}. The Ni^{2+} ions adsorbed on the M-CNCs extremely rapidly, reaching equilibrium adsorption capacity in 5 min. This was mostly caused by the absorbent's strong attraction for metals and the availability and presence of functional groups (**Figure 7**) [52]. As these adsorption sites were gradually occupied, the adsorption rate decreased, possibly due to the electrostatic repulsion between the adsorbed Ni^{2+} cations. In addition, increasing the initial Ni^{2+} concentration of the solution increased the adsorption kinetics and the interaction of Ni^{2+} ions with the adsorption sites, thereby enhancing the adsorption capacity. This result was comparable to the findings of recent studies. Yu et al. used NaSCNCs for Cd^{2+} and Pb^{2+} adsorption, which reached equilibrium within 5 min [43]. Kwat et al. studied the adsorption of Ni^{2+} using *Escherichia coli* biomass and AmberLite IRN150 resin within similar adsorption times [52].

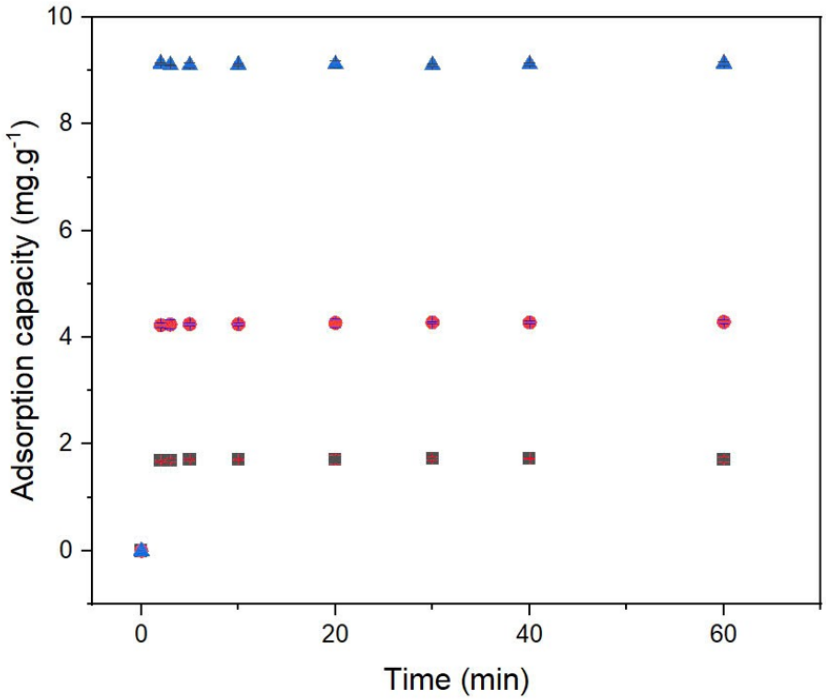

Figure 7: Effect of contact time on Ni^{2+} adsorption by carboxylated cellulose nanocrystal (adsorbent dose = 100 mg, pH = 7, and initial Ni^{2+} concentration = 10 – 40 mg L^{-1}). The square, circle, and

triangle plots represent adsorption capacity within different adsorption times at initial Ni^{2+} concentrations of 10, 20, and 40 mg L^{-1}, respectively.

Adsorption kinetics

The kinetics of Ni^{2+} adsorption on the M-CNCs were investigated using the data obtained from the time-dependent adsorption experiments. Two commonly used kinetic models were applied to analyze the adsorption kinetics: pseudo-first-order and pseudo-second-order models [53,54], which are broadly expressed as

$$\ln(q_e - q_t) = \ln q_e - k_1 \times t, \quad (1)$$

$$\frac{t}{q_t} = \frac{1}{k_2 \times q_e{}^2} + \frac{t}{q_e}, \quad (2)$$

where q_e and q_t (mg g^{-1}) are the adsorption capacities at equilibrium and time t, respectively, and k_1 and k_2 are the apparent first-order model constant (min^{-1}) and apparent second-order model constant (g/mg·min), respectively.

The kinetics of Ni^{2+} adsorption by the M-CNCs are shown in **Table 1**. The results indicated that the adsorption kinetics followed the pseudo-second-order kinetic equation, with the regression coefficient (R^2 = 1) significantly surpassing that of the pseudo-first-order model. Furthermore, the equilibrium adsorption capacity calculated using the kinetic equation (q_{theory}) was comparable to the theoretical equilibrium adsorption capacity (q_{real}) obtained from the pseudo-second-order model, whereas the results from the pseudo-first-order model showed a considerable difference. Therefore, the Ni^{2+} adsorption process fit the pseudo-second-order kinetic model, suggesting that chemical adsorption was the main process for the adsorption of Ni^{2+} ions on the adsorbent. The material surface carried a negative charge (COO^-) and was neutralized by Na^+ ions (using $NaHCO_3$). During adsorption, some Ni^{2+} ions were exchanged with Na^+ ions on the material surface to reach equilibrium, and the time factor affected the adsorption process [55]. This result was similar to those of studies on the adsorption of Ni^{2+} ions on different materials, such as nano alumina–silica [56] and nano bentonite [57].

Table 1: Data of pseudo-first-order model and pseudo-second-order model for Ni^{2+} adsorption on Carboxylated Cellulose Nanocrystal.

Pseudo-first-order kinetics			**Pseudo-second-order kinetics**	
q_{theory} (mg g^{-1})	q_{real} (mg g^{-1})	R^2	q_{real} (mg g^{-1})	R^2
1.734	0.015	0.0026	1.715	0.9999
4.330	0.072	0.5919	4.319	0.9999
9.131	0.012	0.0245	9.119	1

Isothermal adsorption

Adsorption isotherm analysis is important in designing experiments and fabricating adsorbent materials. The Langmuir isotherm model, which describes the monolayer adsorption of ions on an adsorbent at a constant temperature, is [58]

$$\frac{C_e}{q_e} = \frac{1}{q_{max} \times K} + \frac{C_e}{q_{max}}, \quad (3)$$

where q_e is the adsorption capacity at equilibrium (mg g^{-1}), q_{max} is the maximum adsorption capacity (mg g^{-1}), C_e is the adsorbate concentration in the solution at equilibrium (mol L^{-1}), and K is the Langmuir constant (L mg).

The Freundlich equation is an empirical model for adsorption on heterogeneous surfaces, allowing for multilayer adsorption. It is expressed as [58]

$$\ln q_e = \frac{1}{K_F} + \frac{1}{n} \times \ln C_e, \quad (4)$$

where K and n, the Freundlich constants, represent the sorbent's adsorption capacity and intensity, respectively.

The results in **Table 2** show that the Ni^{2+} adsorption isotherm of the M-CNCs followed the Langmuir isotherm equation, with a regression coefficient of 0.998. The maximum Ni^{2+} adsorption capacity of the M-CNCs surface was 9.05 mg g^{-1}. Ni^{2+} adsorbed in a monolayer on the M-CNCs material,

which had a homogeneous surface, with a weak adsorbent–adsorbate interaction. The Ni^{2+} adsorption of the M-CNCs was compared with that of other biosorbents reported in the literature. Their Ni^{2+} adsorption capacity depended on the experimental conditions. The maximum Ni^{2+} adsorption capacity in this study was compared with those in other studies, such as those on ZrO_2-modified nanohybrid cellulose (4.95 mg/g) [59], baker's yeast (9.01 mg g^{-1}) [60], and *Mucor rouxii* mushroom (1.7 mg g^{-1}) [61]. Therefore, the M-CNCs sorbent has a relative adsorption capacity for Ni^{2+}.

Table 2: Data on Freundlich and Langmuir isotherms for Ni^{2+} adsorption on carboxylated cellulose nanocrystal.

Freundlich			**Langmuir**		
K_f	n_f	R^2	q_m	K_L	R^2
0.606	0.42	0.837	9.05	0.08	0.998

Conclusion

We successfully synthesized bleached BFFH through three-step pretreatment and obtained CNCs from the bleached BFFH via acid hydrolysis. According to FE-SEM, the obtained CNCs had a rod-like structure and dimensions ranging from 120 to 200 nm. RSM was used to optimize the CNCs modification process, and the optimal conditions for CNCs surface modification were identified as follows: m_{CNCs} = 3 g, $t_{stirring}$ = 1 h, $V_{NaNO_2}:V_{HNO_3}$ = 5:1, and V_{NaNO_2} = 22.5 mL. FT-IR confirmed the successful isolation of bleached BFFH (through a comparison with commercial MCC) and successful CNCs modification (through the conversion of hydroxyl groups to carboxylates). The adsorption of Ni^{2+} ions by the M-CNCs followed pseudo-second-order kinetics and the Langmuir isotherm model, indicating monolayer adsorption with a maximum capacity of 9.09 mg g^{-1}. Under optimal experimental conditions (1 h adsorption time, 25 mL sample solution, 0.1 g adsorbent mass and pH = 7), the M-CNCs demonstrated a Ni^{2+} ion removal efficiency of approximately 70% from a standard solution. This simple,

easy synthesis method, which uses sustainable resources, positions M-CNCs as promising materials for treating and recovering Ni^{2+} from e-waste. This contributes to the pursuit of sustainable development and net-zero emissions.

Materials and methods

Materials

Analytical-grade nickel, cobalt, and manganese stock solutions (99%; 1000 mg L^{-1} each) and reagents, namely, sodium hydroxide (NaOH), potassium dichromate ($K_2Cr_2O_7$), sodium hydrocarbonate ($NaHCO_3$), and lithium nitrate ($LiNO_3$), were obtained from Merck (Germany). MCC ($(C_6H_{10}O_5)_n$) (99%; Zhanyun, China) served as the comparative adsorbent to assess the performance of synthesized CNCs. In addition, acid solutions and solvents consisting of glacial acetic acid (CH_3COOH), hydrochloric acid (HCl), hydrogen peroxide (H_2O_2, 30%), nitric acid (HNO_3, 68%), sulfuric acid (H_2SO_4, 98%), and absolute ethanol (C_2H_5OH, 99%) were purchased from Merck (Germany). All chemicals used in the experiments were of high purity and used directly as obtained. Distilled water was used throughout the experiments.

Purification of BFFH and extraction of CNCs

Fiber was separated from BFFH, which was sourced from An Giang Province, and subjected to heat treatment. The resulting product was dried at 60 °C, ground into a fine powder, and sieved through a 150 μm sieve.

The BFHH powder was subjected to a three-step treatment process—alkali pretreatment, delignification, and bleaching—to purify cellulose. Fifty grams of powder were stirred in 1000 mL of 1 M NaOH at a fixed temperature of 80 °C for 4 h. The obtained powder underwent wet digestion and dewaxing with a 350 mL CH_3COOH: HCl mixture (100:0.3, v/v) at 60 °C for 3 h to eliminate lignin. Then, the delignified BFFH was bleached using 450 mL of 0.5 M NaOH, 150 mL of H_2O_2 was gradually added, and the mixture was heated at 90 °C. The mixture was further dispersed in 300 mL of 0.5 M NaOH at 80 °C for 8 h.

Following the acid hydrolysis process reported by Nepomuceno et al. [62], 5 g of dried, bleached BFFH was milled, sieved through a 50-mesh screen, and added to 50 mL of a 50 wt.% H_2SO_4 solution under constant stirring at 45 °C for 1 h to yield CNCs. The suspension was diluted by adding cold water and left to settle overnight to decant the supernatant. Afterward, centrifugation was performed at 2000 rpm with deionized water three times to remove excess acid from the remaining suspension. The obtained CNCs were neutralized to a fixed pH with 1 M NaOH and then dried at 70 °C. The dried product was finally milled and sieved through a 100-mesh screen.

Modification of CNCs

In this step, 27 mL of a 1:115 (m/m) $NaNO_2$:HNO_3 solution was added to the milled CNCs, and the mixture was tightly sealed and stirred at 75 °C for 60 min [45]. The reaction was quenched by diluting it with 50 mL of distilled water, followed by decantation to remove the supernatant. This decantation process was repeated two to three times, depending on the weight of the dried CNCs [63]. The solid product was washed with water and centrifuged at 3000 rpm for 10 min until the pH exceeded 4. The suspension was treated with 0.025 M $NaHCO_3$ until pH reached to 7.5, converting the carboxylic acid functional groups (–COOH) to carboxylated functional groups (–COONa), to enhance the dispersion of nanofibers in the aqueous solution and improve metal ion adsorption. Finally, the M-CNCs product was isolated via centrifugation at 3000 rpm for 10 min and washed thoroughly before further use.

Response surface methodology

The CNCs modification process was optimized by implementing a statistical experimental design approach using the software MODDE 5.0 (Sartorius, Göttingen, Germany). A screening design was initially conducted to identify significant factors, and a central composite face (CCF)–centered model design was used to investigate the effects of the CNCs mass (0.1 – 3.0 g), stirring time (1 – 24 h) [45], and $NaNO_2$:HNO_3 ratio (3:5 to optimal value) on the Ni^{2+} adsorption efficiency of the M-CNCs.

Initially, a screening model was adopted to identify and assess the factors that significantly affected adsorption. From this analysis, the variables with notable influence were selected to determine

the optimal conditions for CNCs surface modification using the CCF design. Ultimately, a surface optimization model was used to evaluate and predict these optimal conditions, allowing for the identification of values for the variables that would maximize adsorption efficiency.

Characterization of products from *Borassus flabellifer* fruit husk

The bleached BFFH, CNCs, and M-CNCs were characterized using FT-IR, FE-SEM, and BET analysis. FT-IR analysis was performed using a Spectrum Two FT-IR spectrometer, which has a $LiTaO_3$ detector (at wavenumber of 500 – 4000 cm^{-1}) and attenuated total reflectance accessories. The morphology of the materials was examined using a FE-SEM analysis (Merlin Compact, Carl Zeiss, Jena, Germany), which was performed at 5 kV accelerating voltage and a dual InLensDuo/SE2 detector setup. Prior to analysis, the sample (drop-casted on a clean silicon wafer) was sputter-coated with a thin Pt layer (thickness of 8nm). BET analysis was performed on the samples using a Micromeritics TriStar II Plus surface area analyzer. The quantity of samples used was 0.5 – 1.0 g, and the backfill was nitrogen (99.999%).

Batch adsorption experiments

Various factors influencing Ni (II) adsorption were examined, including the solution pH, adsorbent amount, contact time, and Ni (II) concentration. The liquid-phase volume was maintained at 50 mL. All adsorption mixtures were agitated using a reciprocating shaker (Boeco, Germany) at 250 rpm. Afterward, the suspensions were centrifuged at 3000 rpm for 5 min using a PLC-012 universal centrifuge (Germany) to obtain a clear supernatant. The residual concentration of Ni^{2+} in the supernatant was measured using flame atomic absorption spectroscopy (ICP-6300, Shimadzu, Japan) at a wavelength of 232 nm.

The percentage of removal efficiency (H%) and adsorption capacity (q_e, mg g^{-1}) were calculated according to Eqs. (5) and (6), respectively.

$$H\% = (C_0 - C_e) * C_0 * 100\%, \quad (5)$$

$$q_e = (C_0 - C_e) * V_m, \quad (6)$$

where C_0 and C_e (mg L^{-1}) are the initial and equilibrium concentrations, respectively, of the adsorbate in the solution; V (L) is the volume of the adsorption solution; m (g) is the mass of the adsorbent; and q_e (mg g^{-1}) is the adsorption capacity of the adsorbent at equilibrium, expressed as the amount of adsorbate adsorbed per unit mass of adsorbent.

Acknowledgements

This work was supported by the National Research Foundation of Korea (NRF), grant funded by the Korea government (MSIT) number RS-2023-00219710 and RS-2024-00333541.

References

(1) Yu, M.; Bai, B.; Xiong, S.; Liao, X. *J. Clean. Prod.* **2021**, *321*, 128935. doi:10.1016/j.jclepro.2021.128935

(2) Xie, J.; Huang, K.; Nie, Z.; Yuan, W.; Wang, X.; Song, Q.; Zhang, X.; Zhang, C.; Wang, J.; Crittenden, J. C. *Resour. Conserv. Recycl.* **2021**, *168*, 105261. doi:10.1016/j.resconrec.2020.105261

(3) Coman, V.; Robotin, B.; Ilea, P. *Resour. Conserv. Recycl.* **2013**, *73*, 229–238. doi:10.1016/j.resconrec.2013.01.019

(4) Mashhadikhan, S.; Ebadi Amooghin, A.; Sanaeepur, H.; Shirazi, M. M. A. *Desalination* **2022**, *535*, 115815. doi:10.1016/j.desal.2022.115815

(5) Doyo, A. N.; Kumar, R.; Barakat, M. A. *J. Taiwan Inst. Chem. Eng.* **2023**, *151*, 105095. doi:10.1016/j.jtice.2023.105095

(6) Wu, Z.; Soh, T.; Chan, J. J.; Meng, S.; Meyer, D.; Srinivasan, M.; Tay, C. Y. *Environ. Sci. Technol.* **2020**, *54*, 9681–9692. doi:10.1021/acs.est.0c02873

(7) Akinjokun, A. I.; Petrik, L. F.; Ogunfowokan, A. O.; Ajao, J.; Ojumu, T. V. *Heliyon* **2021**, *7*, e06680. doi:10.1016/j.heliyon.2021.e06680

(8) Beyan, S. M.; Amibo, T. A.; Prabhu, S. V.; Ayalew, A. G. *J. Nanomater.* **2021**, *2021*, 1–12. doi:10.1155/2021/7492532

(9) Abdul Rahman, N. H.; Chieng, B. W.; Ibrahim, N. A.; Abdul Rahman, N. *Polymers (Basel).* **2017**, *9*, 588. doi:10.3390/polym9110588

(10) Amirulhakim, H.; Juwono, A. L.; Roseno, S. *IOP Conf. Ser. Mater. Sci. Eng.* **2021**, *1098*, 062067. doi:10.1088/1757-899X/1098/6/062067

(11) Lu, S.; Ma, T.; Hu, X.; Zhao, J.; Liao, X.; Song, Y.; Hu, X. *J. Sci. Food Agric.* **2022**, *102*, 312–321. doi:10.1002/jsfa.11360

(12) Wang, S.; Zou, Q.; Zhang, L.; Zheng, W.; Huang, X.; Zhang, J. *Ind. Crops Prod.* **2023**, *197*, 116607. doi:10.1016/j.indcrop.2023.116607

(13) Samsalee, N.; Meerasri, J.; Sothornvit, R. *Carbohydr. Polym. Technol. Appl.* **2023**, *6*, 100353. doi:10.1016/j.carpta.2023.100353

(14) Vishnuvarthanan, M.; Dharunya, R.; Jayashree, S.; Karpagam, B.; Sowndharya, R. *Environ. Chem. Lett.* **2019**, *17*, 1429–1434. doi:10.1007/s10311-019-00879-9

(15) Guiso, M. G.; Biesuz, R.; Vilariño, T.; López-García, M.; Rodríguez Barro, P.; Sastre de Vicente, M. E. *Ind. Eng. Chem. Res.* **2014**, *53*, 2251–2260. doi:10.1021/ie402900n

(16) K., R.; T., G.; K., V.; M., S.; P.N., S. *Int. J. Biol. Macromol.* **2019**, *131*, 461–472. doi:10.1016/j.ijbiomac.2019.03.064

(17) Zheng, L.; Zhu, C.; Dang, Z.; Zhang, H.; Yi, X.; Liu, C. *Carbohydr. Polym.* **2012**, *90*, 1008–1015. doi:10.1016/j.carbpol.2012.06.035

(18) Zhang, X.; Xi, C.; Guo, S.; Yan, M.; Lu, Y.; Sun, Z.; Ge, X.; Shen, H.; Ospankulova, G.;

Muratkhan, M.; Kh, K. Z.; Hu, Y.; Li, W. *Ind. Crops Prod.* **2024**, *209*, 118035. doi:10.1016/j.indcrop.2024.118035

(19) Morton, J. F. *Econ. Bot.* **1988**, *42*, 420–441. doi:10.1007/BF02860166

(20) Singh, J. K.; Rout, A. K.; Kumari, K. *Carbohydr. Polym.* **2021**, *262*, 117929. doi:10.1016/j.carbpol.2021.117929

(21) Vengaiah, P. C.; Kaleemullah, S.; Madhava, M.; Mani, A.; Sreekanth, B. *Pharma Innov. J.* **2021**, *10*, 1920–1925

(22) Boopathi, L.; Sampath, P. S.; Mylsamy, K. *Compos. Part B Eng.* **2012**, *43*, 3044–3052. doi:10.1016/j.compositesb.2012.05.002

(23) Rana, A. K.; Frollini, E.; Thakur, V. K. *Int. J. Biol. Macromol.* **2021**, *182*, 1554–1581. doi:10.1016/j.ijbiomac.2021.05.119

(24) Bianchi, M. L.; Crisol, R.; Schuchardt, U. *Bioresour. Technol.* **1999**, *68*, 17–21. doi:10.1016/S0960-8524(98)00075-3

(25) Cui, S.; Zhang, S.; Ge, S.; Xiong, L.; Sun, Q. *Ind. Crops Prod.* **2016**, *83*, 346–352. doi:10.1016/j.indcrop.2016.01.019

(26) Filson, P. B.; Dawson-Andoh, B. E.; Schwegler-Berry, D. *Green Chem.* **2009**, *11*, 1808. doi:10.1039/b915746h

(27) Zhou, Y.; Saito, T.; Bergström, L.; Isogai, A. *Biomacromolecules* **2018**, *19*, 633–639. doi:10.1021/acs.biomac.7b01730

(28) Isogai, A.; Saito, T.; Fukuzumi, H. *Nanoscale* **2011**, *3*, 71–85. doi:10.1039/C0NR00583E

(29) Saito, T.; Kimura, S.; Nishiyama, Y.; Isogai, A. *Biomacromolecules* **2007**, *8*, 2485–2491. doi:10.1021/bm0703970

(30) Seta, F. T.; An, X.; Liu, L.; Zhang, H.; Yang, J.; Zhang, W.; Nie, S.; Yao, S.; Cao, H.; Xu, Q.;

Bu, Y.; Liu, H. *Carbohydr. Polym.* **2020**, *234*, 115942. doi:10.1016/j.carbpol.2020.115942

(31) Song, K.; Ji, Y.; Wang, L.; Wei, Y.; Yu, Z. *J. Clean. Prod.* **2018**, *196*, 1169–1175. doi:10.1016/j.jclepro.2018.06.128

(32) El Achaby, M.; El Miri, N.; Hannache, H.; Gmouh, S.; Trabadelo, V.; Aboulkas, A.; Ben Youcef, H. *Cellulose* **2018**, *25*, 6603–6619. doi:10.1007/s10570-018-2047-1

(33) O'Connell, D. W.; Birkinshaw, C.; O'Dwyer, T. F. *Bioresour. Technol.* **2008**, *99*, 6709–6724. doi:10.1016/j.biortech.2008.01.036

(34) Bezerra, M. A.; Santelli, R. E.; Oliveira, E. P.; Villar, L. S.; Escaleira, L. A. *Talanta* **2008**, *76*, 965–977. doi:10.1016/j.talanta.2008.05.019

(35) Şener, M.; Reddy, D. H. K.; Kayan, B. *Ecol. Eng.* **2014**, *68*, 200–208. doi:10.1016/j.ecoleng.2014.03.024

(36) Rathika, R.; Byung-Taek, O.; Vishnukumar, B.; Shanthi, K.; Kamala-Kannan, S.; Janaki, V. *e-Polymers* **2018**, *18*, 287–295. doi:10.1515/epoly-2017-0215

(37) Gapsari, F.; Purnowidodo, A.; Hidayatullah, S.; Suteja, S. *J. Mater. Res. Technol.* **2021**, *13*, 1305–1315. doi:10.1016/j.jmrt.2021.05.049

(38) Wardani, R. K.; Holilah, H.; Bahruji, H.; Abdul Hamid, Z. A.; Suprapto, S.; Jalil, A. A.; Nugraha, R. E.; Prasetyoko, D. *Sustain. Chem. Pharm.* **2024**, *39*, 101583. doi:10.1016/j.scp.2024.101583

(39) Zhang, H.; Wu, J.; Zhang, J.; He, J. *Macromolecules* **2005**, *38*, 8272–8277. doi:10.1021/ma0505676

(40) Wang, Y.; Wei, X.; Li, J.; Wang, F.; Wang, Q.; Chen, J.; Kong, L. *Fibers Polym.* **2015**, *16*, 572–578. doi:10.1007/s12221-015-0572-1

(41) Coseri, S.; Biliuta, G.; Zemljič, L. F.; Srndovic, J. S.; Larsson, P. T.; Strnad, S.; Kreže, T.; Naderi, A.; Lindström, T. *RSC Adv.* **2015**, *5*, 85889–85897. doi:10.1039/C5RA16183E

(42) Tang, Y.; Petropoulos, K.; Kurth, F.; Gao, H.; Migliorelli, D.; Guenat, O.; Generelli, S. *Biosensors* **2020**, *10*. doi:10.3390/bios10090125

(43) Yu, X.; Tong, S.; Ge, M.; Wu, L.; Zuo, J.; Cao, C.; Song, W. *J. Environ. Sci. (China)* **2013**, *25*, 933–943. doi:10.1016/S1001-0742(12)60145-4

(44) Poda, A.; Anderson, A.; Ashurst, W. R. *Appl. Surf. Sci.* **2010**, *256*, 6805–6813. doi:10.1016/j.apsusc.2010.04.093

(45) Oyewo, O. A.; Mutesse, B.; Leswifi, T. Y.; Onyango, M. S. *J. Environ. Chem. Eng.* **2019**, *7*. doi:10.1016/j.jece.2019.103251

(46) Khuri, A. I.; Mukhopadhyay, S. *WIREs Comput. Stat.* **2010**, *2*, 128–149. doi:10.1002/wics.73

(47) Beck, S.; Bouchard, J.; Berry, R. *Biomacromolecules* **2012**, *13*, 1486–1494. doi:10.1021/bm300191k

(48) Afroze, S.; Sen, T. K. *Water. Air. Soil Pollut.* **2018**, *229*. doi:10.1007/s11270-018-3869-z

(49) Ogbu, I. **2017**, No. June

(50) Chen, H.; Sharma, S. K.; Sharma, P. R.; Chi, K.; Fung, E.; Aubrecht, K.; Keroletswe, N.; Chigome, S.; Hsiao, B. S. *Cellulose* **2021**, *28*, 8611–8628. doi:10.1007/s10570-021-04057-5

(51) Wang, H.; Friedrich, B. *J. Sustain. Metall.* **2015**, *1*, 168–178. doi:10.1007/s40831-015-0016-6

(52) Kwak, I. S.; Won, S. W.; Choi, S. B.; Mao, J.; Kim, S.; Chung, B. W.; Yun, Y. S. *Korean J. Chem. Eng.* **2011**, *28*, 927–932. doi:10.1007/s11814-010-0441-y

(53) Charazińska, S.; Burszta-Adamiak, E.; Lochyński, P. *Rev. Environ. Sci. Bio/Technology* **2022**, *21*, 105–138. doi:10.1007/s11157-021-09599-5

(54) Zhan, W.; Xu, C.; Qian, G.; Huang, G.; Tang, X.; Lin, B. *RSC Adv.* **2018**, *8*, 18723–18733. doi:10.1039/C8RA02055H

(55) Barquilha, C. E. R.; Cossich, E. S.; Tavares, C. R. G.; da Silva, E. A. *Environ. Sci. Pollut. Res.*

2019, *26*, 11100–11112. doi:10.1007/s11356-019-04552-0

(56) Chatterjee, A.; Basu, J. K.; Jana, A. K. *Powder Technol.* **2019**, *354*, 792–803. doi:10.1016/j.powtec.2019.06.035

(57) Ahmed, A. M.; Ayad, M. I.; Eledkawy, M. A.; Darweesh, M. A.; Elmelegy, E. M. *Heliyon* **2021**, *7*, e06315. doi:10.1016/j.heliyon.2021.e06315

(58) Gebreslassie, Y. T. *J. Anal. Methods Chem.* **2020**, *2020*, 1–11. doi:10.1155/2020/7384675

(59) Khan, S. B.; Alamry, K. A.; Marwani, H. M.; Asiri, A. M.; Rahman, M. M. *Compos. Part B Eng.* **2013**, *50*, 253–258. doi:10.1016/j.compositesb.2013.02.009

(60) Padmavathy, V. *Bioresour. Technol.* **2008**, *99*, 3100–3109. doi:10.1016/j.biortech.2007.05.070

(61) Yan, G.; Viraraghavan, T. *Water Res.* **2003**, *37*, 4486–4496. doi:10.1016/S0043-1354(03)00409-3

(62) Nepomuceno, N. C.; Seixas, A. A. A.; Medeiros, E. S.; Mélo, T. J. A. *J. Solid State Chem.* **2021**, *302*. doi:10.1016/j.jssc.2021.122372

(63) Sharma, P. R.; Joshi, R.; Sharma, S. K.; Hsiao, B. S. *Biomacromolecules* **2017**, *18*, 2333–2342. doi:10.1021/acs.biomac.7b00544